Full title: Augmented reality guided laparoscopic liver resection: a phantom study with intraparenchymal tumours

Running head: Quantitative assessment of augmented reality

List of authors: Mathieu Ribeiro, M.D. (1, 2), Yamid Espinel, Ph.D. (2), Navid Rabbani, Ph.D. (2), Bruno Pereira, Ph.D. (3), Adrien Bartoli, Ph.D. (2), Emmanuel Buc, M.D. Ph.D. (1, 2)

Author affiliations

(1) Department of Digestive and Hepatobiliary Surgery, Hospital Estaing, CHU de Clermont-Ferrand, 1 Place Lucie et Raymond Aubrac, 63003, Clermont-Ferrand, France

(2) UMR6602, Endoscopy and Computer Vision Group, Faculté de Médecine, Institut Pascal, Bâtiment 3C, 28 place Henri Dunant, 63000, Clermont-Ferrand, France.

(3) Biostatistics unit (DRCI), University Hospital Clermont-Ferrand, 63000 Clermont-Ferrand

Corresponding author

Emmanuel Buc, M.D., Ph.D.

Department of Digestive and Hepatobiliary Surgery, Estaing Hospital

University of Clermont-Auvergne

1, place Lucie et Raymond Aubrac

63003 Clermont-Ferrand Cedex

Tel: +(33)473752389

Email: ebuc@chu-clermontferrand.fr

Abstract

Background. Augmented reality (AR) in laparoscopic liver resection (LLR) can improve intrahepatic navigation by creating a virtual liver transparency. Our team has recently developed Hepataug, an AR software that projects the invisible intrahepatic tumours onto the laparoscopic images and allows the surgeon to localise them precisely. However, the accuracy of registration according to the location and size of the tumours, as well as the influence of the projection axis, have never been measured. The aim of this work was to measure the 3D tumour prediction error of Hepataug.

Materials and methods. Eight 3D virtual livers were created from the CT scan of a healthy human liver. Reference markers with known coordinates were virtually placed on the anterior surface. The virtual livers were then deformed and 3D printed, forming 3D liver phantoms. After placing each 3D phantom inside a pelvitrainer, registration allowed Hepataug to project virtual tumours along two axes: the laparoscope axis and the operator port axis. The surgeons had to point the centre of eight virtual tumours per liver with a pointing tool whose coordinates were precisely calculated.

Results. We obtained 128 pointing experiments. The average pointing error was 29.4 ± 17.1 mm and 9.2 ± 5.1 mm for the laparoscope and operator port axes respectively ($p=0.001$). The pointing errors tended to increase with tumour depth (correlation coefficients greater than 0.5 with $p<0.001$). There was no significant dependency of the pointing error on the tumour size for both projection axes.

Conclusion. Tumour visualisation by projection toward the operating port improves the accuracy of AR guidance and partially solves the problem of the 2D visual interface of monocular laparoscopy. Despite a lower precision of AR for tumours located in the posterior part of the liver, it could allow the surgeons to access these lesions without completely mobilising the liver, hence decreasing the surgical trauma.

Key words. Laparoscopic; hepatectomy; augmented reality; projection; pointing; accuracy

Introduction

Augmented reality (AR) is currently developing in laparoscopic liver resection (LLR), as it enables overlaying the patient's liver virtual 3D model, reconstructed from the preoperative images, on the laparoscopic images, which can help the surgeon see the internal liver structures by virtual transparency. Compared to intraoperative laparoscopic ultrasound (LUS), AR has tremendous advantages. First, the information is directly visible on the laparoscopy screen, over the entire liver and without limit on the field of exploration. Second, AR can be used in real-time, without interrupting the surgical procedure, and the visual information given by AR is easy to interpret without specific skills, user-independent, and, consequently, reproducible [1]. The challenges of AR in LLR arise from the high deformability of the liver parenchyma and the fact that the entire liver surface is not always visible in the laparoscope's field of view, with modification of the landmarks due to gravity, pressure of the pneumoperitoneum, breathing and cardiac movements [2].

Our team has recently developed an AR software for LLR called Hepataug. This software uses a semi-automatic deformable registration to overlay the preoperative virtual 3D model on the laparoscopic images. Hepataug allows the projection of hidden tumours onto the laparoscopic liver images, which can help the surgeon to locate them precisely and to improve the resection margins [3,4]. Teams working on AR in hepatic surgery have mainly focused on the virtual to real registration stage and the quantitative evaluation of its spatial accuracy. Systems for AR in 3D laparoscopic surgery reach an accuracy of about 13.9 mm [5] and of about 8.73 mm [6]. Our system Hepataug for AR in 2D laparoscopy reaches an accuracy of about 9 mm [7], which is on par with the other systems. In contrast, the overall guidance error, evaluating the AR system's ability to guide the surgeon, was not quantified in the literature. Some studies discuss the issue of visualisation, mainly to reveal the guidance problems arising with monocular

laparoscopes [7–10]. However, changing the projection axis was not brought up as a solution. Related work includes coupling an AR software with visual and audio markers to further assist the surgeon's actions [11]. While promising, this does not directly solve the misguidance problem.

This article proposes the pointing error, which is a type of error that quantifies the ability of a setup to guide the surgeon to an intraparenchymal tumour. In specific, given that the surgeon uses AR guidance to aim at the tumour, the pointing error measures how far from the tumour will they pass. The pointing error encompasses the 3D tumour prediction error and the means used to display AR guidance. This error follows the same principle as the target positioning lateral error [12], as they both measure the normal distance between the tool axis and the target's centre. We chose this name because it measures the distance between a pointing device that the surgeon uses to indicate where they believe the tumour is and the true location of the tumour. We use the pointing error to show that the projection of the tumour toward the camera along the camera axis, as is done in previous work, is a major source of misguidance. We propose instead a double projection system, where the tumour is projected first to the liver surface towards the operator port and only then to the camera along the camera axis. Concretely, we first evaluate Hepataug's accuracy using 3D phantoms and also give a quantitative evaluation of the pointing error. We then compare the pointing errors when the projection is done with the proposed double projection system, which clearly shows that it outperforms and should be used in the majority of AR guidance systems.

Materials and methods

Liver phantoms:

Eight 3D printed phantoms were created in eight different simulated deformed configurations. A healthy control subject that gave his consent was chosen to generate the liver phantoms. Since it was a healthy subject and no invasive procedures were involved, IRB considered that review was not necessary for this study. Eight 3D printed phantoms were then created in eight different simulated deformed configurations. For each phantom, we proceeded as follow (figure 1a):

Step 1 - L0: virtual 3D base model. Based on CT images from the control subject, a unique virtual 3D liver model was created. In order to control the 3D reconstruction bias, the liver segmentation was performed by a senior surgeon who manually segmented the liver in each slice of the CT using the MITK software [13]. Intrahepatic structures (vessels, incidental benign cysts and tumours) were not reconstructed. The resulting 3D model is called L0 (figure 1b).

Step 2 - L1: virtual 3D model with tumours. Eight spheres, representing tumours, were added to L0 using the Blender software [14]. The tumour diameters were selected from 10 to 20 mm, as it forms a common range of tumour size, and positioned in random typical locations of the liver (figure 1c). Tumours #1 to #4 were located in the right lobe of the liver, while tumours #5 to #8 were located in the left lobe. Some of the tumours were positioned in posterior and/or deep areas of the liver, that are usually the most difficult to identify. Concretely, tumours #1, #2, #3, #6, and #7 were located in the liver's posterior side, while tumours #4, #5, and #8 were located in its anterior side.

Step 3 - L2: virtual 3D model with tumours and reference markers. We virtually added 555 reference markers with known coordinates on the anterior surface of the L1 model, which will be used to later find the pose of the L1 model in space (figure 1d). The pose is defined as the relative position and orientation with respect to other objects and devices in our experimental

setup. The reference markers can be recognised from an image of the phantom and used to estimate its pose.

Step 4 - L3: deformed L2 model. The L2 model underwent 8 different random deformations using the Abaqus software [15], generating 8 new models which we called the L3 models (figure 1e). The imposed forces were adjusted to simulate the effects of the pneumoperitoneum and of the surgical instruments on the liver. Specifically, liver #1 simulates a deformation caused by a tool mildly lifting the right lobe. Liver #2 is deformed by pushing the right lobe downwards. Liver #3 is deformed by pushing the right lobe backwards. Liver #4 is deformed by lifting the right lobe's posterior part. Liver #5 is deformed by lifting the whole right lobe. Liver #6 is deformed by lifting the right lobe and pushing it backwards. Liver #7 is deformed by lifting the left lobe's posterior part. Liver #8 is deformed by lifting the right and left lobes simultaneously. The deformations were chosen at a reasonable amplitude to remain close to the intraoperative conditions of LLR. The deformed L3 models are shown in figure 2. The eight tumours added in step 2 (L1) followed the deformations.

Step 5 – L4: final 3D printed phantoms. The eight L3 models were printed using a 3D printer (Ultimaker 2 Extended) with rigid, *i.e.*, non-deformable, material (polylactic acid) to build eight physical phantoms, which we called the L4 models. The physical L4 phantoms are similar to their L3 virtual 3D model twins to a very good extent (figure 1f).

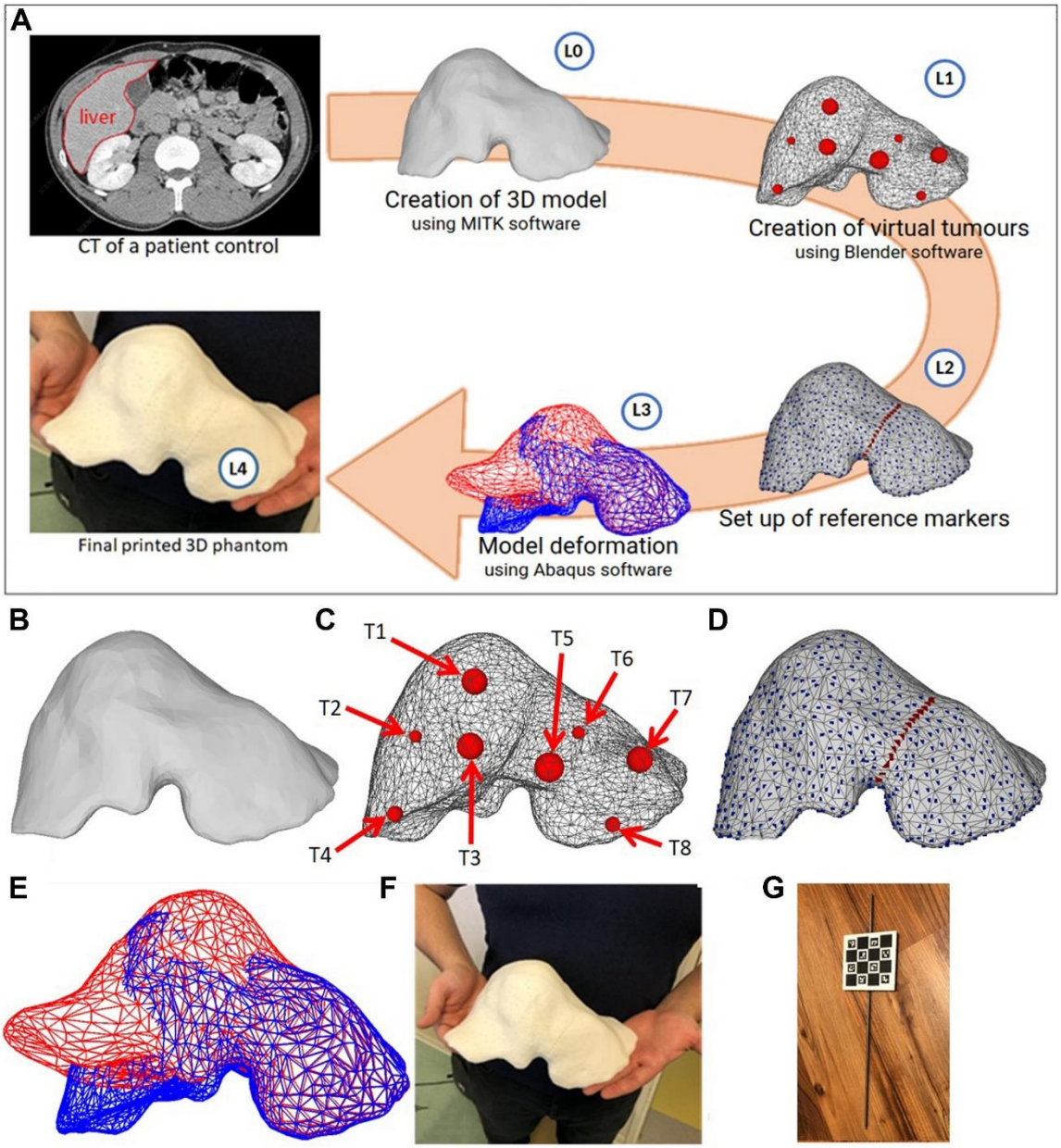

Figure 1: the successive steps used to create the L4 liver phantom. a) global scheme; b) virtual 3D model of the real patient liver (L0); c) virtual 3D model with the 8 added tumours and their corresponding locations (L1); d) virtual 3D model with reference markers (L2); e) superposition of two virtual models, before deformation (model in blue) and after deformation by Abaqus (model in red) (L3); f) 3D printing of L3 (L4); g) the pointing device with its ChArUco pattern.

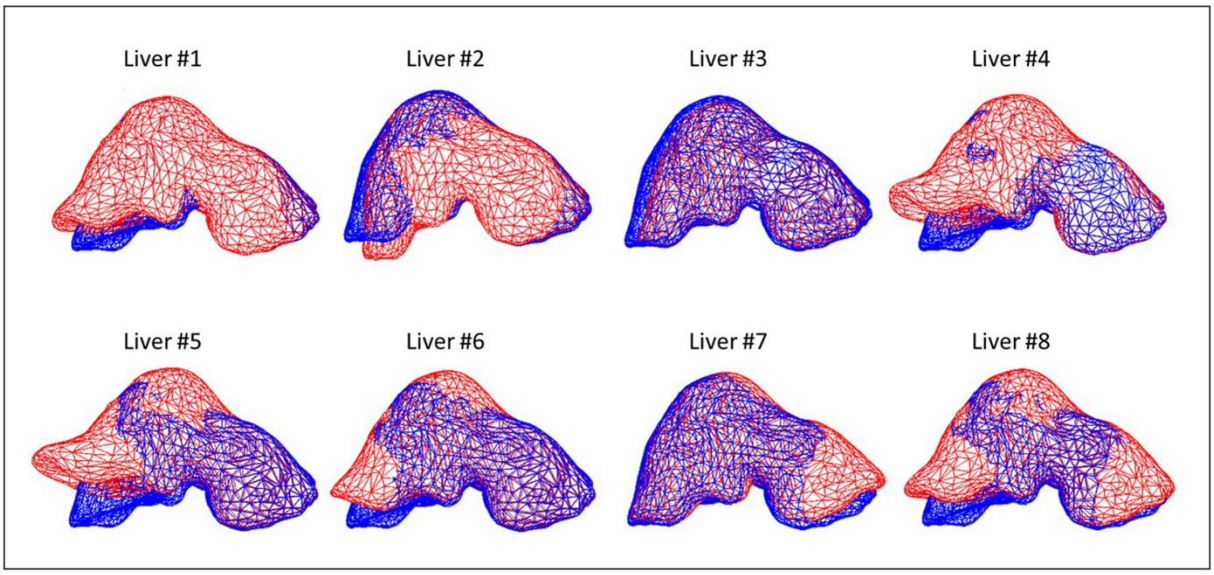

Figure 2: the eight deformed L3 models used in our experiments. The model in blue corresponds to the undeformed L1 model. The models in red are the deformed L3 models.

Pointing tool:

The aim of the experiment was to point the augmented virtual tumours to calculate the accuracy of the pointing via the pointing error. For this purpose, we developed a specific pointer, which is a 50 cm rigid rod of 5 mm diameter with a sharp tip at its distal end and an attached flat surface on its proximal end hosting a printed ChArUco pattern [16] (figure 1g). The ChArUco pattern allows us to calculate the pose of the pointing tool, including the coordinates of its tip and its direction.

Experimental surgical installation:

A covered laparoscopy training box, namely pelvic trainer, was used to simulate the operative conditions of LLR. The pelvic trainer was open on both lateral sides so that the L4 phantoms could be inserted and placed. A remote camera (Sony Alpha 6000 24.3 megapixels) was used to record the whole scene and to take the necessary photographs. We used it as a 3D metrology device that can find the pose of the liver phantoms and the pointing axis of the pointing tool.

A laparoscope (Karl Storz Image 1S) with Xenon 300 light source was inserted through one of the pelvic trainer ports. Before each experiment, both the laparoscope and remote camera were calibrated to find their internal calibration parameters. These are the parameters needed to model the lens and imaging sensor of each of these two imaging devices. The calibration was done using the Photoscan Lens software [17]. Concretely, a checkerboard pattern was filmed using both cameras. Then, images of both video sequences were imported in the Photoscan Lens software suite, which estimated the calibration parameters. Throughout the experiment, all the devices (pelvic trainer, experimental liver phantom, camera and laparoscope) were fixed to limit parasitic movements (figure 3). Concretely, the pelvic trainer and the experimental liver phantom were stabilised on a table, the camera was installed on a tripod to ensure perfect stability, and the laparoscope was fixed using an articulated surgical arm.

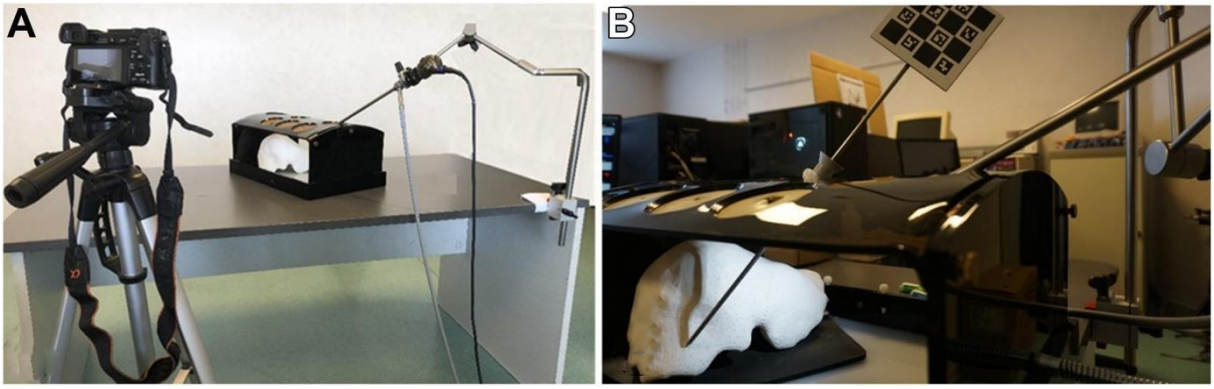

Figure 3: experimental setup with all elements fixed. a) General view of the experimental setup; b) view in experimental condition with the pointing tool.

Hepataug registration:

Hepataug is designed to augment the preoperative virtual 3D model on the laparoscopic images. As the liver may have been deformed in laparoscopic images compared to preoperative imaging, Hepataug uses deformable registration to align the 3D model over the laparoscopic image. The L1 model (the virtual 3D model with tumours but without deformation) was used as the preoperative model, together with a laparoscopic image of an L4 deformed model.

Hepataug uses semi-automatic registration and the AR procedure was completed after three successive phases: first, the anatomical landmarks, namely the upper silhouette, inferior ridge contour and falciform ligament, were marked on both the L1 virtual model and the L4 laparoscopic image. Second, Hepataug performed registration, to deform the L1 model and align it over the L4 laparoscopic image [7,18]. Finally, after registration, Hepataug overlaid the tumours and their projection axis. The projection can be done towards the laparoscope or the operator port of the pelvic trainer using the proposed double projection system. The registrations were done for every image separately; we thus did not track the liver between images to update registration.

Pointing, photography and data treatment:

The surgeon was asked to point each projection of the tumours at the liver surface using the pointer (figure 4). The experiment was repeated for each tumour (8 tumours), for each L4 phantoms (8 livers) and according to 2 different types of projection (projection towards the laparoscope and projection towards the operator port following the double projection system) (figure 5). The coordinates of the operator port were calculated in relation to the laparoscope, as they are required for the first projection in the double projection system. A photograph was taken for each pointing experiment, which covered the L4 phantom and the pointing tool. The pose of the L4 phantom and of the pointing tool were calculated for each of these photographs.

The liver pose was computed as follows: the reference markers on the L4 phantom were marked manually in the photograph. As the position of these markers is known in the corresponding L3 model, the pose could be computed with an algorithm called EPnP [19]. The pose of the pointing tool was also calculated using this algorithm, from the automatic detection of the ChArUco pattern. The virtual position of the tumours was known from their creation of the liver L3 model. Then, with the estimated pose of the L4 phantom and the pointing tool, we

could calculate the pointing error, defined as the distance between the pointing axis and the centre of the virtual tumour.

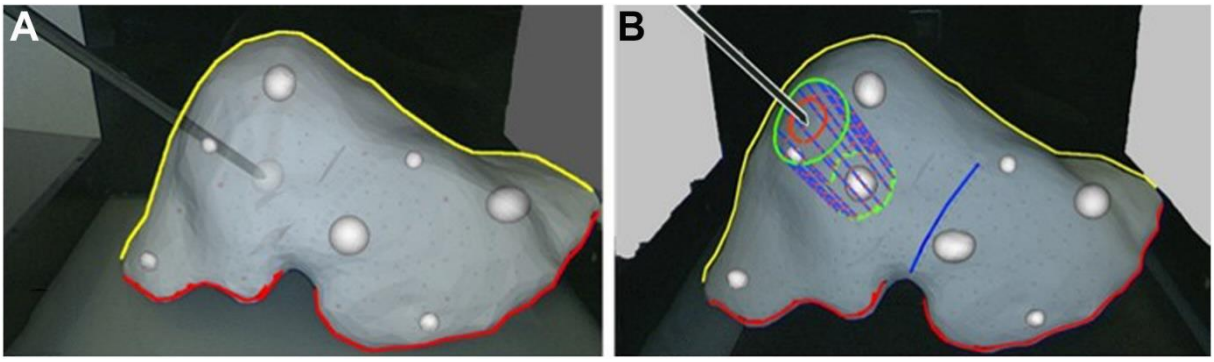

Figure 4: virtual 3D model before (a) and after (b) projection of a tumour to the liver surface, toward an operative port. The closed red curve is the tumour projection and the closed green curve is the projection of the 1 cm oncologic margins around the tumour. The anatomic landmarks used for registration are the yellow curve representing the upper liver silhouette, the red curve representing the inferior ridge and the blue curve representing the falciform ligament.

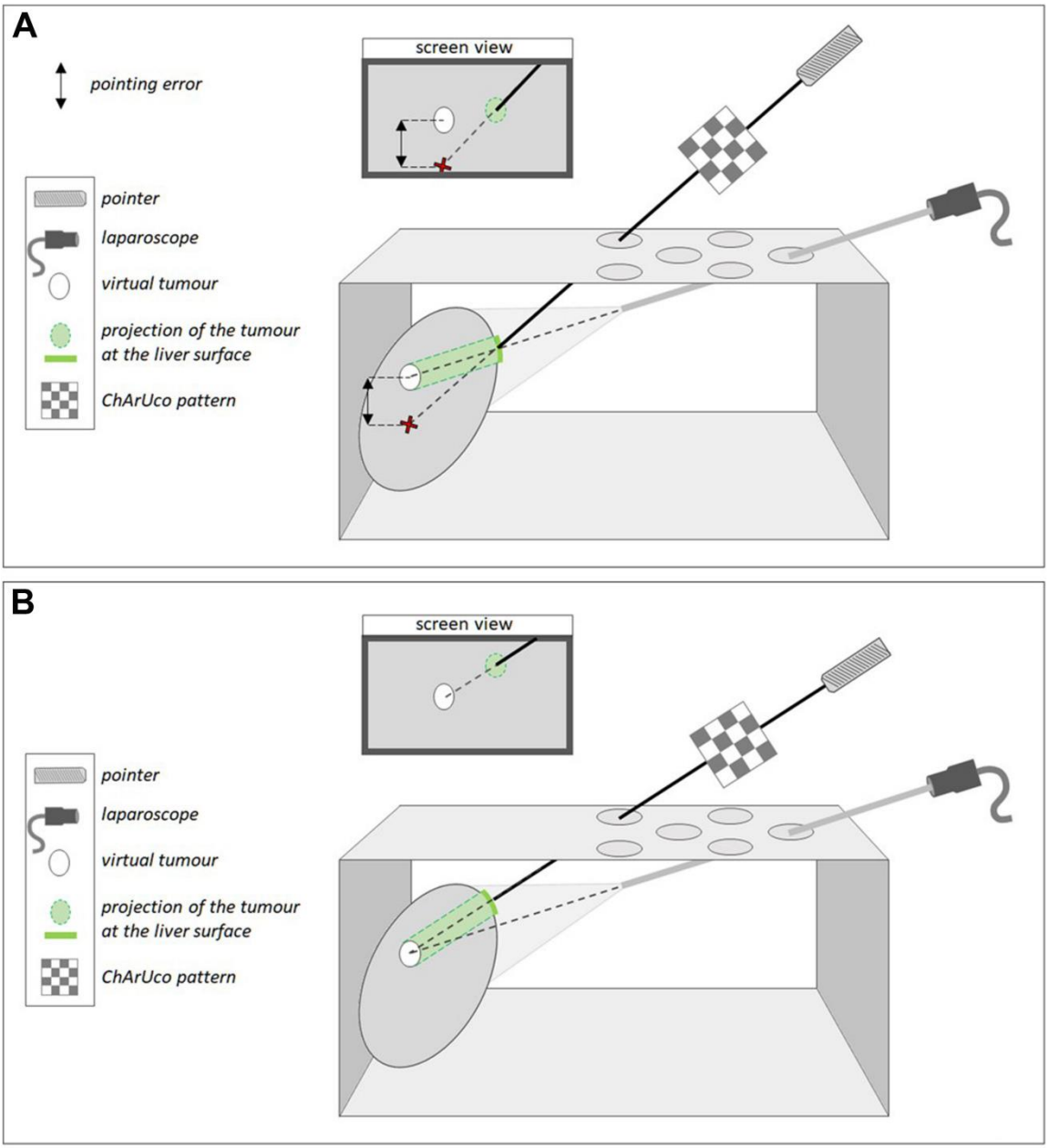

Figure 5: superposition of the liver structures at its surface with projection to the laparoscope axis (a) and to the operative port (b).

Statistics:

Continuous data were presented as the mean and standard deviation (SD). The assumption of normality was assessed using the Shapiro-Wilk test. A logarithmic transformation of the dependent variable was applied where appropriate. The pointing error was compared between projection towards the operator port and projection towards the laparoscope by a random-effects model suitable to take into account subject variability, owing to the presence of 8 tumours in each phantom. The relationship between the tumour size and the accuracy of the registration was analysed with a similar statistical approach. The relationship between the pointing error and tumour depth was analysed with the Spearman correlation coefficient. Statistical analysis was performed using Stata software (version 15, StataCorp, College Station, US). The tests were two-sided with a type I error set at 5%.

Results

Eight liver phantoms with eight tumours in each phantom were tested, for a total of 128 pointing experiments. The average pointing error of the 8 tumours for each phantom is given in table 1. The pointing error was significantly higher when the projection was performed towards the laparoscope axis (p=0.001). The mean pointing errors according to the tumour size are listed in table 2. There was no significant difference of pointing errors according to the size of the tumour, whatever the axis of projection. The pointing errors were also investigated according to the depth of the tumours. Considering that tumour #8 was the most superficial and that tumour #2 was the deepest, the pointing errors tended to increase with tumour depth (correlation coefficients greater than 0.5 with $p<0.001$) (table 3, figure 6).

Table 1. Mean pointing error for the eight tumors in each L4 phantom.

L4 phantoms	**L4-01**	**L4-02**	**L4-03**	**L4-04**	**L4-05**	**L4-06**	**L4-07**	**L4-08**	**Mean ± SD**
Mean pointing error (mm) *Projection toward the operator port*	6.3	7.9	10.3	11.8	11.9	7.2	9.3	9.1	9.2 ± 5.1
Mean pointing error (mm) *Projection toward the laparoscope*	23.5	24.5	29.6	31.9	34.3	29.5	32.4	29.5	29.4 ± 17.1

Table 2. Mean pointing errors according to tumor size in the eight L4 phantoms.

Tumor ID	**T1**	**T3**	**T5**	**T7**	**Mean ± SD**	**T2**	**T4**	**T6**	**T8**	**Mean ± SD**	***P value***
Tumor size (mm)	**20**	**20**	**20**	**20**		**10**	**10**	**10**	**10**		
Mean pointing error (mm) *Projection toward the operator port*	12.2	10.5	4.9	7.7	**8.8** ± 3.9	16.3	10.3	6.6	5.2	**9.6** ± 6.2	**0.53**

Mean pointing error (mm) *Projection toward the laparoscope*	35.8	48.8	21.3	20.7	**31.5** ± 12.6	58.5	10.4	29.6	10.4	**27.2** ± 20.7	**0.30**

Bold highlights the difference of the mean value of the pointing error between projection towards the laparoscope and projection towards the operator port.

Table 3. Mean pointing errors according to tumor depth in the eight L4 phantoms.

Tumor ID	**T8**	**T4**	**T5**	**T7**	**T6**	**T3**	**T1**	**T2**	***Correlation coefficient (P value)***
Deep from the liver surface (mm)	**12**	**18**	**20**	**25**	**33**	**48**	**56**	**94**	
Mean pointing error (mm) *Projection toward the operator port*	5.2	10.3	4.9	7.7	6.6	10.5	12.2	16.3	0.56 (<0.001)
Mean pointing error (mm) *Projection toward the laparoscope*	10.4	10.4	21.3	20.7	29.6	48.8	35.4	58.5	0.92 (<0.001)

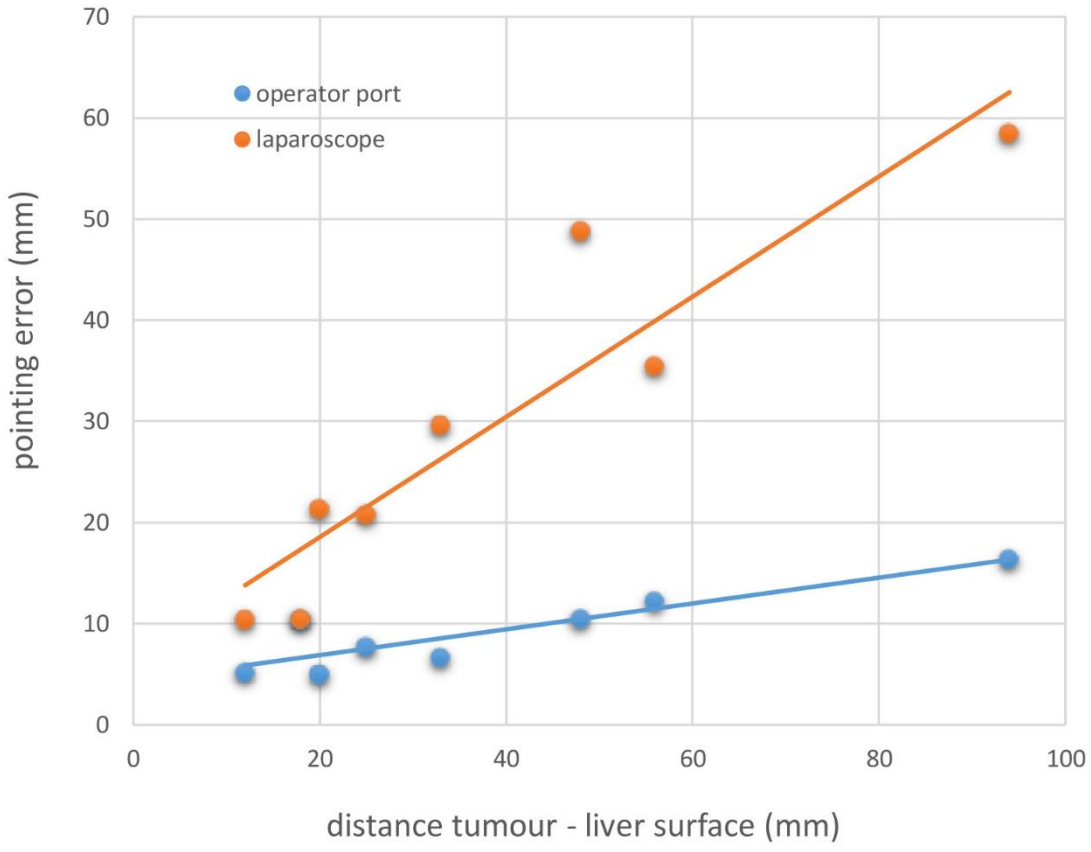

Figure 6: comparison of the pointing error between laparoscope axis and operator port projection of the tumours, according to tumour depth.

Evaluation of uncertainty in our methodology:

To estimate the uncertainty in our methodology in determining pointing errors, we performed an experiment designed to exclude the influence of Hepataug. We used a single liver phantom (L4-01) for the main experiment, but L3-01 was used as the 3D model for AR instead of L1-01. As L3-01 has exactly the same shape as L4-01, deformable registration was not required and a simple alignment between L3-01 and a laparoscopic image of L4-01 became sufficient for AR. Consequently, the obtained pointing error was only due to the uncertainty in our methodology and did not include the Hepataug registration error. The average pointing error when the tumours were projected towards the operator port and the laparoscope port was respectively of 10.4 and 27.6 mm (table 4), which strongly supports the conclusions involving the complete system with Hepataug.

Table 4. Pointing errors for each tumor after exclusion of Hepataug registration by processing the L3-01 virtual model and the L4-01 phantom.

Tumor ID of L4-01	**T1**	**T2**	**T3**	**T4**	**T5**	**T6**	**T7**	**T8**	**Mean**
Pointing error (mm) *Projection toward the operator port*	11.4	14.2	12.8	10.2	7.2	12.7	7.2	7.33	10.4
Pointing error (mm) *Projection toward the laparoscope*	26.4	60.5	36.8	11.6	21.8	34.6	15.8	13.1	26.7

Discussion

AR in laparoscopic liver surgery is a developing technique with the continuous emergence of several software systems. This enthusiasm can be explained by the ability of AR to tackle the challenge of increasing the rate of mini-invasive approaches around the world while preserving the oncologic quality of the resection and the safety of the procedure. Some teams have put their AR software to preliminary clinical tests but have only studied quantitatively the tumour prediction error, without taking into account the surgeon's expectations, especially for AR visualisation [9,18]. Indeed, the few clinical studies that have taken into account visualisation and surgeon's experience were purely qualitative [3, 20–22]. Our present study addresses this issue. First, we showed that projecting the tumours along the axis of the laparoscope was a major source of misguidance, which increases with the tumour depth. In contrast, projecting along the axis of the operator port to the liver surface consistently improved guidance, with a pointing error of approximately 9 mm. This is consistent with previous computer studies on Hepataug [7,18]. More specifically, we showed that the pointing error increases for posterior and inferior tumours. We showed that the deeper the tumour in the liver parenchyma, the more defective the RA guidance, given that a direct projection of the tumour to the laparoscope is used, which was suspected in other studies [6,21]. Several studies that have tested AR software on *ex-vivo* human or animal livers have thus underestimated the guidance error. This is because ex-vivo organs flatten considerably along the anteroposterior axis and are therefore not representative of the intraoperative conditions, with all tumours being at shallow depth. In our experiments we found that the accuracy of AR guidance substantially degrades for the deepest tumours, the most distant ones from the liver surface. The posterior and non-visible part of the liver in laparoscopic AR remains a major problem yet unsolved, and the missing data from this part of the liver causes imprecisions on the 3D tumour prediction. This strengthens the interest to locate the ports in space during laparoscopic surgery, in order to project the AR towards one

or more operator ports to improve its visualisation and guidance precision. It would be interesting to define the position of the different ports according to their use (camera, operator, assistant) at the beginning of the procedure.

Interestingly, the pointing error is not affected by the tumour size. This result was expected because the way the error is measured is relative to the tumour centre, regardless of their size. This shows an advantage of AR over LUS, for which the difficulty to identify the tumour centre increases with the tumour size.

In our clinical practice we use AR in laparoscopic liver resection to guide and confirm intraoperative US findings, and to identify tumours that have become invisible after neoadjuvant chemotherapy. We use AR only for tumours smaller than 5 cm that can be treated by non-anatomical (wedge) resection, because large tumours require anatomical resection for which hepatectomies are performed in scissural or glissonian planes far from the tumour margin. However, a different clinical application of our study could be radiofrequency ablation (RFA), which is an alternative ablative technique to surgery. RFA is performed using a specific needle of diameter depending on the tumour size, which penetrates the tumour at its centre percutaneously or intraoperatively. Currently, LUS-guided RFA is the gold standard but remains imprecise, especially in deep tumours. Our procedure of pointing using AR has analogies with the RFA LUS-guided procedure, which could thus form a clinical application of an AR system originally developed for laparoscopic liver surgery. Furthermore, small or subcapsular tumours can be invisible in patients with macronodular cirrhosis because the liver surface is not smooth and the rigid surface of the LUS probe can thus not follow the irregularities of the capsule, yielding strong artefacts. In contrast, our work demonstrates that AR guidance to superficial tumours is very reliable, which could be of rapid interest in the identification of tumours on cirrhotic livers.

Our study has limitations. AR in laparoscopic surgery with a monocular camera raises the concern of the loss of depth data on the 2D screen. This is however alleviated by the proposed double projection system. There does not yet exist a consensus for the best projection system for AR visualisation, whether on 2D or 3D laparoscopes. Our double projection system will require validation from other teams before its acceptance. During the experiments, all the devices were fixed, which differs from real intraoperative conditions and could modify the interpretation of the results. However, we fixed the devices to limit the parasitic movements that could interfere with the targeting assessment, considering that liver tracking was neither used nor assessed in this study.

Another limitation is the error margin related to the experimental setup. Indeed, the experimental sequence with pointing with rigid registration using the virtual L3-01 model and its real twin, the L4-01 phantom, showed an average pointing error of 10.4 mm. Because the 3D tumour prediction error is expected to be much smaller, we also expected the pointing error to be much smaller, close to 0 mm. This discrepancy may be explainable in part by other error sources related to the experimental setup (camera calibration and pose computation). However, our team has already characterised these errors in previous work [23]: they were found to be of an order of magnitude lower than the measured pointing error in the present study. The pointing error can thus be imparted for its largest part to the user perception and interpretation, hence to the performance of how visual guidance is concretely achieved by AR. It seems to be high regarding the small size of the tumours, but the aim of this work was, first, to find the best projection axis for tumour pointing (camera or operator), and second, to standardise the quantitative assessment of the pointing error through a reproducible method, forming a basis to improve AR algorithms.

Conclusion

AR systems can bring considerable assistance for the analysis, preoperative planning and localisation of liver tumours in laparoscopic resection. Accuracy must be continuously improved, which is especially important for deep posterior tumours. Nonetheless, the guidance error is reasonable and would be compatible with several clinical use cases.

Further work is needed in two main directions. First, to understand the error sources. The development of 3D laparoscopy through robotic surgery will probably reduce several error sources. Second, to confirm the optimal tumour projection system that, as shown in this study, is a crucial part of an AR system. The development of intraoperative liver tracking to allow continual AR will also probably vastly improve tumour depth perception in both 2D and 3D laparoscopy.

Acknowledgments: none

Disclosures:

Dr. Mathieu Ribeiro: no conflicts of interest or financial ties to disclose

Dr. Yamid Espinel: no conflicts of interest or financial ties to disclose

Dr. Navid Rabbani: no conflicts of interest or financial ties to disclose

Dr. Bruno Pereira: no conflicts of interest or financial ties to disclose

Pr. Adrien Bartoli: no conflicts of interest or financial ties to disclose

Pr. Emmanuel Buc: no conflicts of interest or financial ties to disclose

All the authors disclose the use of AI and AI-assisted technologies in the writing process.

References

1. Ntourakis D, Memeo R, Soler L, Marescaux J, Mutter D, Pessaux P (2016) Augmented Reality Guidance for the Resection of Missing Colorectal Liver Metastases: An Initial Experience. World J Surg 40:419–426. https://doi.org/10.1007/s00268-015-3229-8

2. Hostettler A, Nicolau SA, Rémond Y, Marescaux J, Soler L (2010) A real-time predictive simulation of abdominal viscera positions during quiet free breathing. Progress in Biophysics and Molecular Biology 103:169–184. https://doi.org/10.1016/j.pbiomolbio.2010.09.017

3. Bertrand LR, Abdallah M, Espinel Y, Calvet L, Pereira B, Ozgur E, Pezet D, Buc E, Bartoli A (2020) A case series study of augmented reality in laparoscopic liver resection with a deformable preoperative model. Surg Endosc 34:5642–5648. https://doi.org/10.1007/s00464-020-07815-x

4. Adballah M, Espinel Y, Calvet L, Pereira B, Le Roy B, Bartoli A, Buc E (2022) Augmented reality in laparoscopic liver resection evaluated on an ex-vivo animal model with pseudo-tumours. Surg Endosc 36:833–843. https://doi.org/10.1007/s00464-021-08798-z

5. Thompson S, Schneider C, Bosi M, Gurusamy K, Ourselin S, Davidson B, Hawkes D, Clarkson MJ (2018) In vivo estimation of target registration errors during augmented reality laparoscopic surgery. Int J Comput Assist Radiol Surg 13:865–874. https://doi.org/10.1007/s11548-018-1761-3

6. Luo H, Yin D, Zhang S, Xiao D, He B, Meng F, Zhang Y, Cai W, He S, Zhang W, Hu Q, Guo H, Liang S, Zhou S, Liu S, Sun L, Guo X, Fang C, Liu L, Jia F (2020) Augmented reality navigation for liver resection with a stereoscopic laparoscope. Comput Methods Programs Biomed 187:105099. https://doi.org/10.1016/j.cmpb.2019.105099

7. Espinel Y, Özgür E, Calvet L, Le Roy B, Buc E, Bartoli A (2020) Combining Visual Cues with Interactions for 3D-2D Registration in Liver Laparoscopy. Ann Biomed Eng 48:1712–1727. https://doi.org/10.1007/s10439-020-02479-z

8. Chen L, Tang W, John NW, Wan TR, Zhang JJ (2018) SLAM-based dense surface reconstruction in monocular Minimally Invasive Surgery and its application to Augmented Reality. Computer Methods and Programs in Biomedicine 158:135–146. https://doi.org/10.1016/j.cmpb.2018.02.006

9. Collins T, Chauvet P, Debize C, Pizarro D, Bartoli A, Canis M, Bourdel N (2017) A System for Augmented Reality Guided Laparoscopic Tumour Resection with Quantitative Ex-vivo User Evaluation. In: Peters T, Yang G-Z, Navab N, Mori K, Luo X, Reichl T, McLeod J (eds) Computer-Assisted and Robotic Endoscopy. Springer International Publishing, Cham, pp 114–126

10. Ozgur E, Lafont A, Bartoli A (2017) [POSTER] Visualizing In-Organ Tumors in Augmented Monocular Laparoscopy. In: 2017 IEEE International Symposium on Mixed and Augmented Reality (ISMAR-Adjunct). IEEE, Nantes, France, pp 46–51

11. De Paolis LT, De Luca V (2019) Augmented visualization with depth perception cues to improve the surgeon's performance in minimally invasive surgery. Med Biol Eng Comput 57:995–1013. https://doi.org/10.1007/s11517-018-1929-6

12. Widmann G, Stoffner R, Sieb M, Bale R (2009) Target registration and target positioning errors in computer-assisted neurosurgery: proposal for a standardized reporting of error assessment. Int. J. Med. Robotics Comput. Assist. Surg., 5: 355-365. https://doi.org/10.1002/rcs.271

13. Wolf I, Vetter M, Wegner I, Böttger T, Nolden M, Schöbinger M, Hastenteufel M, Kunert T, Meinzer H-P (2005) The Medical Imaging Interaction Toolkit. Medical Image Analysis 9:594–604. https://doi.org/10.1016/j.media.2005.04.005

14. Zdziebko P, Holak K (2021) Synthetic Image Generation Using the Finite Element Method and Blender Graphics Program for Modeling of Vision-Based Measurement Systems. Sensors 21:6046. https://doi.org/10.3390/s21186046

15. Idkaidek A, Jasiuk I (2015) Toward high-speed 3D nonlinear soft tissue deformation simulations using Abaqus software. J Robotic Surg 9:299–310. https://doi.org/10.1007/s11701-015-0531-2

16. Hu D, DeTone D, Chauhan V, Spivak I, Malisiewicz T (2019) Deep ChArUco: Dark ChArUco Marker Pose Estimation

17. Agisoft LLC (2023) Agisoft Metashape. https://www.agisoft.com/.

18. Özgür E, Koo B, Le Roy B, Buc E, Bartoli A (2018) Preoperative liver registration for augmented monocular laparoscopy using backward-forward biomechanical simulation. Int J Comput Assist Radiol Surg 13:1629–1640. https://doi.org/10.1007/s11548-018-1842-3

19. Lepetit V, Moreno-Noguer F, Fua P (2009) EPnP: An Accurate O(n) Solution to the PnP Problem. Int J Comput Vis 81:155–166. https://doi.org/10.1007/s11263-008-0152-6

20. Le Roy B, Ozgur E, Koo B, Buc E, Bartoli A (2019) Augmented reality guidance in laparoscopic hepatectomy with deformable semi-automatic computed tomography alignment (with video). J Visc Surg 156:261–262. https://doi.org/10.1016/j.jviscsurg.2019.01.009

21. Golse N, Petit A, Lewin M, Vibert E, Cotin S (2021) Augmented Reality during Open Liver Surgery Using a Markerless Non-rigid Registration System. J Gastrointest Surg 25:662–671. https://doi.org/10.1007/s11605-020-04519-4

22. Marescaux J, Rubino F, Arenas M, Mutter D, Soler L (2004) Augmented-reality-assisted laparoscopic adrenalectomy. JAMA 292:2214–2215. https://doi.org/10.1001/jama.292.18.2214-c

23. Rabbani N, Calvet L, Espinel Y, Le Roy B, Ribeiro M, Buc E, Bartoli A (2022) A methodology and clinical dataset with ground-truth to evaluate registration accuracy quantitatively in computer-assisted Laparoscopic Liver Resection. Computer Methods in Biomechanics and Biomedical Engineering: Imaging & Visualization 10:441–450. https://doi.org/10.1080/21681163.2021.1997642